Title:

Clinical and immunological signatures of severe COVID-19 in previously healthy patients with clonal hematopoiesis

Authors:

Chang Kyung Kang[1,*], Baekgyu Choi[2,*], Sugyeong Kim[3], Seongwan Park[2], Soon Ho Yoon[4], Dohoon Lee[5], Andrew J. Lee[2], Yuji Ko[2], Euijin Chang[1], Jongtak Jung[1,6], Pyoeng Gyun Choe[1], Wan Beom Park[1], Eu Suk Kim[1,6], Hong Bin Kim[1,6], Nam Joong Kim[1], Myoung-don Oh[1], Suk-jo Kang[2], Kyuho Kang[7], Sun Kim[8,9], Hogune Im[3], Joohae Kim[10], Yong Hoon Lee[11], Jaehee Lee[11], Ji Yeon Lee[10,†], Joon Ho Moon[11,†], Kyoung-Ho Song[1,6,†], Youngil Koh[1,3,†], Inkyung Jung[2,†]

Affiliations:

[1]Department of Internal Medicine, Seoul National University College of Medicine, Seoul 03080, Republic of Korea.

[2]Department of Biological Sciences, Korea Advanced Institute of Science and Technology (KAIST), Daejeon 34141, Republic of Korea.

[3]Genome Opinion Inc., Seoul 04799, Republic of Korea

[4]Department of Radiology, Seoul National University College of Medicine, Seoul 03080, Republic of Korea.

[5]Bioinformatics Institute, Seoul National University, Seoul 08826, Republic of Korea

[6]Department of Internal Medicine, Seoul National University Bundang Hospital, Seongnam 13620, Republic of Korea.

[7]Department of Biology, Chungbuk National University, Cheongju, 28644, Republic of Korea

[8]Department of Computer Science and Engineering, College of Engineering, Seoul National University, Seoul 08826, Republic of Korea

[9]Interdisciplinary Program in Bioinformatics, College of Natural Sciences, Seoul National University, Seoul 08826, Republic of Korea

[10]Division of Pulmonary and Critical Care Medicine, Department of Internal Medicine, National Medical Center, Seoul 04564, Republic of Korea

[11]Department of Internal Medicine, Kyungpook National University Hospital, School of Medicine, Kyungpook National University, Daegu 41944, Republic of Korea

[*] These authors contributed equally to this work

[†] Correspondence to Ji Yeon Lee (fulgeo@nmc.or.kr), Joon Ho Moon (jhmoon@knu.ac.kr), Kyoung-Ho Song (khsongmd@gmail.com), Youngil Koh (snuhgo01@gmail.com), and Inkyung Jung (ijung@kaist.ac.kr)

Abstract

Identifying additional risk factors for COVID-19 severity in numerous previously healthy patients without canonical clinical risk factors remains challenging. In this study, we investigate whether clonal hematopoiesis of indeterminate potential (CHIP), a common aging-related process that predisposes various inflammatory responses, may exert COVID-19 severity. We examine the clinical impact of CHIP in 143 laboratory-confirmed COVID-19 patients. Both stratified analyses and logistic regression including the interaction between canonical risk factors and CHIP show that CHIP is an independent risk factor for severe COVID-19, especially in previously healthy patients. Analyses of 60,310 single-cell immune transcriptome profiles identify distinct immunological signatures for CHIP (+) severe COVID-19 patients, particularly in classical monocytes, with a marked increase in pro-inflammatory cytokine responses and potent IFN-γ mediated hyperinflammation signature. We further demonstrate that the enhanced expression of CHIP (+) specific IFN-γ response genes is attributed to the CHIP mutation-dependent epigenetic reprogramming of poised or bivalent *cis*-regulatory elements. Our results highlight a unique immunopathogenic mechanism of CHIP in the progression of severe COVID-19, which could be extended to elucidate how CHIP contributes to a variety of human infectious diseases.

20 **Main Text:**

21 **Introduction**

22 A pandemic of coronavirus disease-19 (COVID-19) , an emerging infectious disease caused by
23 severe acute respiratory syndrome-coronavirus-2 (SARS-CoV-2), has been being a global
24 health threat of the century[1,2]. Epidemiologic data revealed that about 20% of patients
25 underwent severe or critical course[3]. Although many clinical risk factors for severe illness
26 including older age, comorbidities such as diabetes mellitus or hypertension, and morbid
27 obesity have been found[4,5], we could still only partly explain the development of severe
28 COVID-19. Indeed, there have been numerous cases of severe COVID-19 from previously
29 healthy adults[6,7].

30 Clinical deteriorations such as acute respiratory distress syndrome or intensive care
31 unit admission most commonly occur at around the 10th day of illness[8,9], when the viral loads
32 are declining after the early peak[10,11]. This temporal discrepancy suggests immunological
33 phenomenon may play an important role in the progression of COVID-19. High levels of
34 circulating pro-inflammatory cytokines[12], aberrant hyperactivation of cytotoxic lymphocytes[13]
35 or their infiltration in vital organs[14], or dysregulated monocytes and macrophages[15] have been
36 proposed as mechanisms for pathologic immune responses in severe COVID-19.

37 Clonal hematopoiesis of indeterminate potential (CHIP) refers to a population of
38 immune cells with acquired gene mutations, but without fulfilling diagnostic criteria for a
39 hematologic malignancy[16]. As a majority of the genes associated with CHIP including
40 *DNMT3A*, *TET2*, and *ASXL1* are involved in epigenetic regulation, CHIP may have a wide
41 range of effects on immune function through altered chromatin activities[17]. There is growing
42 evidence supporting a role for the CHIP mutations in altered immune function through effector
43 cells such as monocytes/macrophages and their dysregulated cytokine/chemokine expression,

44 which account for the increased risk of cardiovascular disease in individuals with CHIP[18-21].
45 Since immunopathogenesis of such an adverse outcome of CHIP largely shares that of severe
46 COVID-19, we hypothesized that CHIP might contribute to the progression of COVID-19 with
47 its unique immune signature. Although recent reports describe the association between
48 acquired mutations in hematopoietic cells such as CH and severe COVID-19[22,23], there has
49 been a controversy on the clinical impact of CHIP in COVID-19[23-25]. However, if there exists
50 a distinct CHIP-related clinical deterioration mechanism of COVID-19, tailored therapeutics
51 could be of help to salvage these patients.

52 In this study, to determine the clinical significance of CHIP in COVID-19 severity,
53 especially in previously healthy adults, we analyzed thorough clinical, radiological, and
54 laboratory characteristics of patients with COVID-19. In addition, we explored immune
55 signatures using single-cell RNA expression data according to the presence of CHIP to suggest
56 how CHIP attributes to the immunologic responses in severe COVID-19. Lastly, since the
57 majority of mutations in CHIP are related to epigenetic regulators of DNA methylation and
58 heterochromatin formation, we investigated CHIP mutation dependent dysregulated epigenetic
59 gene regulation mechanisms involved in CHIP-specific immunopathogenesis.

Results

Impact of CHIP on severe COVID-19 in previously healthy patients

A total of 143 laboratory-confirmed COVID-19 patients were analyzed in this study (Fig. 1a). Among those, 34 patients had CHIP (23.8%, Supplementary Table 1). *DNMT3A* (13 variants) was the most common mutated gene, followed by *TET2* (7 variants) and *ASXL1* (5 variants). Clinical characteristics were retrospectively reviewed using electronic medical record (EMR) systems of each institution. It included age, sex, body mass index, presence of comorbidities, details of oxygen and medical therapy, duration of hospital stay, and in-hospital mortality. Serial laboratory findings including complete blood count with differential count and chemistries were also collected. Cases with the highest ordinal scale 3 (need for supplemental oxygen therapy via nasal cannula) or more were classified as severe COVID-19, while others were classified with mild ones[3].

Baseline characteristics of these patients are shown in Supplementary Table 1. Median (interquartile range [IQR]) ages were 73 (61—81) and 65 (50—75) years in those with or without CHIP, respectively (Student's *t*-test, $P < 0.001$), as consistent with a common aging-related property of CHIP. The presence of CHIP appears to contribute to COVID-19 severity as severe COVID-19 tended to be more frequent in patients with CHIP than those without, while the difference was statistically not significant (25/34, 73.5% vs. 65/109, 59.6%, Chi-squared test, $P = 0.143$).

To precisely examine the clinical impact of CHIP in patients with COVID-19, we conducted a hierarchical clustering analysis for baseline characteristics and examined the distribution of CHIP among clusters (Fig. 1b). All continuous clinical information was transformed into a range of 0 to 1 using a logistic function, and comorbidity status was dichotomized into 0 and 1 for absence and presence (see Methods). Patients were grouped into

two main clusters, A and B. They mainly comprised severe and mild cases, respectively, since cluster A had significantly higher ordinal scores, peak serum C-reactive protein level, and peak chest X-ray score than cluster B (Unpaired t-test, $P < 0.001$) (Fig. 1c). Cluster A was subdivided into three clusters, A1, A2, and A3 with their own comorbidity status (Fig. 1d). Cluster A1 was characterized by the presence of hypertension, while cluster A3 was a DM-enriched group.

Interestingly, cluster A2 tended to have a higher rate of CHIP than the others in cluster A (Fisher's exact test, $P = 0.074$), while it had significantly lower BMI (median [IQR], 20.8 [17.8—23.1] vs. 23.0 [21.7—26.1]; Student's *t*-test, $P = 0.005$) and lower rate of DM (0/18, 0% vs. 22/51, 43.1%; Fisher's exact test, $P = 0.001$) or hypertension (0/18, 0% vs. 40/51, 78.4%; Fisher's exact test, $P < 0.001$) (Fig. 1d and Supplementary Table 2). However, age distribution was not statistically different (Fisher's exact test, $P = 0.662$).

The presence of a particular type of severe cases uniquely enriched by CHIP without canonical risk factors such as DM, hypertension, and high BMI led us to hypothesize that CHIP may contribute to severe COVID-19 in its own way. An additional hierarchical clustering with DM, hypertension, and CHIP information in all severe patients (Ordinal scale >=3) also supported our hypothesis since it showed that CHIP was clustered together (Extended Data Fig. 1).

To test the statistical significance of the impact of CHIP on COVID-19 severity in previously healthy patients, we stratified the entire patients by the presence of any of the canonical risk factors such as DM, hypertension, and BMI $\geq$ 30.0. When adjusted with age and gender, the risk of severe COVID-19 was significantly higher in CHIP (+) patients than in CHIP (-) ones in canonical risk factor-absent subgroup (adjusted odds ratio [95% confidence interval], 14.8 [1.3—164.1]; logistic regression $P = 0.028$; Table 1). Multivariate analysis

107 including the interaction between canonical risk factors and CHIP revealed that CHIP was an
108 independent risk factor for severe COVID-19 (adjusted odds ratio [95% confidence interval],
109 10.7 [1.1—100.7], logistic regression $P = 0.038$, Table 2). The results of the patients clustering
110 and the statistical evidence indicate that CHIP is an independent risk factor for severe COVID-
111 19, especially in previously healthy patients.

112

113 **Distinct immune signatures in CHIP (+) severe COVID-19**

114 We next sought to identify distinct immune signatures for severe COVID-19 according to the
115 presence of CHIP. To this end, a total of 60,310 high-quality single-cell transcriptome
116 profiles of peripheral blood mononuclear cells (PBMCs) generated by 10x Genomics single-
117 cell RNA-seq (scRNA-seq) platform were integrated from healthy donors (n=4), severe
118 influenza (n=5), CHIP (-) mild COVID-19 (n=5), CHIP (-) severe COVID-19 (n=3), and
119 CHIP (+) severe COVID-19 (n=6) specimens (Supplementary Table 3 and 4, see Methods),
120 with an average of 6,100 unique molecular identifies (UMIs), representing 1,400 genes. The
121 reproducibility and quality were ensured (Extended Data Fig. 2a-c)[26]. Based on t-distributed
122 stochastic neighbor embedding (t-SNE) of transcriptome profiles, 24 subgroups were derived.
123 Assigning cell types with previously annotated marker genes (Extended Data Fig. 2d-e, see
124 Methods)[26], we focused on 9 major immune cell types, including IgG^+ B cell, IgG^- B cell,
125 $CD4^+$ T cell, naïve $CD4^+$ T cell, $CD8^+$ T cell, $CD8^+$ memory T cell, natural killer (NK) T cell,
126 classical monocyte, and non-classical monocyte in subsequent analyses (Fig. 2a). Non-
127 immune cells such as platelets, red blood cells (RBCs), and uncategorized small cell
128 populations were excluded. Notably, the proportion of monocytes was markedly increased,
129 particularly in CHIP (+) severe COVID-19 patients (K–S test, P=3.49e-3) (Extended Data

130 Fig. 2f-g), consistent with the known impact of CHIP with increased myeloid cell
131 population[27].

132 In terms of transcriptome profiles at the cell-type resolution, as expected, most immune
133 cell types originating from COVID-19 were clustered together when compared to influenza
134 (Fig. 2b). Interestingly, those from severe COVID-19 were subdivided according to the
135 presence of CHIP (Fig. 2b). To investigate relevant biological functions that establish such
136 unique host immune responses in CHIP (+) severe COVID-19, we identified up-regulated
137 genes specific to CHIP (+) severe COVID-19 compared to healthy normal control, influenza,
138 CHIP (-) mild COVID-19, and CHIP (-) severe COVID-19, respectively, using MAST
139 algorithm (Extended Data Fig. 3a)[28]. Regardless of both normal and disease control groups,
140 tumor necrosis factor (TNF-α)/NF-kB and interferon-gamma (IFN-γ) responses were
141 commonly enriched in up-regulated genes in CHIP (+) severe COVID-19 (Extended Data Fig.
142 3b). A noticeable enrichment of CHIP (+) up-regulated genes was observed in classical
143 monocytes (Extended Data Fig. 3c).

144 To further investigate the unique immune signatures at the individual immune cell-
145 type resolution, we conducted gene set enrichment analysis (GSEA) for differentially
146 expressed genes between CHIP (+) and CHIP (-) severe COVID-19. Based on cytokine-
147 responsive gene sets originated from each cytokine treated cells (LINC L1000 ligand
148 perturbation analysis in Enrichr) (see Methods)[29], strong IL-1β and TNF-α responses were
149 observed in both CHIP (+) and CHIP (-) severe COVID-19 compared to healthy normal control
150 (Fig. 2c). However, direct comparison between CHIP (+) and CHIP (-) severe COVID-19
151 revealed that immune responses in classical monocytes were strongly skewed towards CHIP
152 (+) patients (Fig. 2d), while other cell types such as T cells, B cells or non-classical monocytes
153 did not show such trend (Fig. 2e-g, Extended Data Fig. 4a-e). Taken together, CHIP (+) patients

154 under COVID-19 infection present unique host immune responses, particularly in classical
155 monocytes.

156

157 **Classical monocyte-mediated hyperinflammation in CHIP (+) severe COVID-19**

158 To examine how the presence of CHIP attributes to the immunologic responses in classical
159 monocytes, we focused on analyzing 445 up- and 417 down-regulated CHIP (+) specific genes.
160 CHIP (+) up-regulated genes demonstrated enrichment with inflammation cytokine responses,
161 such as IL-1β compared to CHIP (-) (Mann-Whitney's U test, *P*=3.24e-2, IL-1β) (Fig. 3a).
162 Other COVID-19 representative interleukins such as IL-6, IL-10 and IL-15 were also elevated
163 in CHIP (+) severe COVID-19. (Fig. 3b)[30]. Notably, CHIP (+) up-regulated genes were
164 strongly related to both type I and II interferon (IFN) responses (Mann-Whitney's U test,
165 *P*=1.08e-3, IFN-γ; *P*=3.97e-3, IFN-α). We previously proposed that a group of genes involved
166 in type I IFN-induced TNF-α mediated hyperinflammation by abolishing the tolerance effects
167 of TNF-α (Class 1 gene in Park *et al.*[31]) in monocyte has a critical role in promoting
168 hyperinflammation of COVID-19[26]. Consistently, the CHIP (+) up-regulated genes presented
169 a modest enrichment with the Class I genes (Fig. 3c), partly explaining the hyperinflammation
170 signature of CHIP (+). However, other inflammatory TLR-induced genes regardless of TNF-α
171 tolerization (Class II and III genes in Park *et al.*[31]) were extremely biased to CHIP (+) up-
172 regulated genes, postulating the presence of additional classical monocyte driven responses
173 exacerbating the inflammation signatures in CHIP (+).

174

175 **IFN-γ mediated hyperinflammation in CHIP (+) severe COVID-19 revealed by a**
176 **pseudotime analysis**

177 Intriguingly, IFN-γ response was notably high in CHIP (+) up-regulated genes (Fig. 3a). As a
178 high level of IFN-γ has been reported as an indicator of severe COVID-19[8,32,33], we
179 hypothesized that IFN-γ response could attribute to hyperinflammation signatures of classical
180 monocytes in CHIP (+) patients. We first determined the association between IFN-γ response
181 and COVID-19 severity in CHIP (+) by conducting pseudotime analysis using the specimens
182 collected twice from one patient to exclude innate individual biases (Fig. 4a) (see Methods).
183 After ordering cells along with the trajectory analysis, we allocated the annotation of high and
184 low inflammation clusters based on inflammatory signatures termed in MsigDB Hallmark 2020
185 (Fig. 4b). We found that IFN-γ response genes were significantly enriched in a high
186 inflammation group of CHIP (+), even more potent than that of CHIP (-) (Fig. 4c).

187 Recent mouse and scRNA-seq comparison studies have highlighted the immuno-
188 pathogenic contribution of IFN-γ in severe COVID-19 as demonstrated by IFN-γ induced
189 inflammatory macrophage phenotype and synergistic effect of IFN-γ and TNF-α[34,35].
190 Consistently, in our analysis, CHIP (+) specific genes were significantly enriched by pro-
191 inflammatory M1-like macrophage-specific genes obtained from two independent studies[36]
192 [37](Fig. 4d and Extended Data Fig. 5a) and associated with up-regulated genes by co-treatment
193 of TNF-α and IFN-γ (Fig. 4e)[35]. Such enrichment suggests that CHIP (+) severe COVID-19
194 patients are representative cases that could be explained by previously discovered IFN-γ
195 mediated disease exacerbating mechanism. For a treatment perspective, we noticed that spleen
196 tyrosine kinase (Syk) inhibitor, which is known to reduce the expressions of interferon-
197 stimulated genes[38], may be an effective molecule for the intervention of CHIP (+) up-regulated
198 genes (Paired t-test, P=0.042) (Extended Data Fig. 5b). Taken together, IFN-γ response is
199 thought to be a main source of the hyperinflammation immune signature in CHIP (+) severe
200 COVID-19.

201

202 ***DNMT3A* mutation-specific hypo-DMRs are linked to IFN-γ response genes**

203 Next, we sought to identify mechanisms by which IFN-γ response genes are up-regulated
204 explicitly in CHIP (+) COVID-19 patients. Considering mutations of multiple epigenetic
205 regulators such as *DNMT3A*, *TET2*, and *ASXL1* in CHIP, we hypothesized that altered
206 chromatin activity of *cis*-regulatory elements might exert CHIP-specific gene expression. To
207 test our hypothesis, we identified 2,348 differentially methylated regions (DMRs) in acute
208 myeloid leukemia (AML) patients carrying *DNMT3A* mutations (see Methods)
209 (Supplementary Table 5)[39]. In support of our hypothesis, these DMRs were highly overlapped
210 with putative regulatory elements (Fisher's exact test, $P<0.001$, Proximal to the promoter;
211 $P<0.001$, Distal regulatory element) (Fig. 5a) (see Methods). As exemplified in *FOXO3* and
212 *NFIL3,* known IFN response genes*,* CHIP (+) up-regulated genes were also more closely
213 located to the hypo-DMRs (Fig. 5b, Extended Data fig. 6).

214 As many *cis*-regulatory elements are known to target genes over large genomic
215 distances[40], we performed *in situ* Hi-C experiments on $CD14^{++}/CD16^{-}$ classical monocytes of
216 two healthy donors to precisely annotate target genes of CHIP-dependent DMRs (see Methods).
217 With ~500M long-range chromatin interactions over 15kb genomic distance, we defined
218 significant long-range chromatin contacts using covNorm in 10kb resolution (see Methods)[41].
219 Using this information, as illustrated in *RBPJ* and *CXCL2* genes (Fig. 5c-d), we revealed that,
220 in total, around 33% of CHIP-specific up-regulated genes, denoted as 'linked genes', were
221 associated with hypo-DMRs either in proximal (within 15kb) or long-range chromatin
222 interactions (over 15kb but less than 2Mb) (Fig. 5e). Notably, those linked genes were more
223 enriched by both type I and II IFN response genes compared to the remaining up-regulated
224 genes (Mann-Whitney's U test, P=2.50e-3, IFN-γ; P =3.97e-3, IFN-α) (see Methods) (Fig. 5f).

225 Regarding high inflammation cluster in pseudotime analysis, we revealed that IFN-γ response
226 genes largely overlap by hypo-DMRs linked genes (Mann-Whitney's U test, P =1.08e-3, IFN-
227 γ) (Fig. 5g). Our results strongly support that CHIP-dependent altered chromatin activities are
228 associated with putative *cis*-regulatory elements of IFN-γ response genes, which may establish
229 unique gene expression profiles in CHIP patients during immune responses.

230

231 **Activation of poised and bivalent *cis*-regulatory elements primes IFN-γ response genes**

232 To further characterize CHIP-specific hypo-DMRs, we examined the enrichment of four
233 representative histone modification marks including histone H3 4th lysine mono-methylation
234 (H3K4me1), tri-methylation (H3K4me3), 27th lysine acetylation (H3K27ac), and tri-
235 methylation (H3K27me3) of primary human classical monocyte[42,43]. When comparing DMRs
236 to randomly selected genomic regions, hypo-DMRs were mostly marked by H3K27me3 in the
237 primary human classical monocytes, while hyper-DMRs were enriched by H3K27ac as an
238 indicator of active regulatory elements (Fig. 6a-b). However, interestingly, a subset of hypo-
239 DMRs, linking to CHIP (+) up-regulated genes, were also significantly co-occupied by
240 H3K4me1 and H3K4me3 peaks compared to the unlinked hypo-DMRs (Fisher's exact test,
241 P<0.001, H3K4me1; P<0.001, H3K4me3; P =2.37e-2, H3K27ac) (Fig. 6c-d). Such co-
242 exhibition of inactive and active chromatin signatures indicates that the regulatory elements of
243 CHIP (+) up-regulated genes have shifted from poised or bivalent status to an active chromatin
244 state through the process of CHIP dependent hypo-DNA methylation. To test this possibility,
245 we annotated chromatin states of linked hypo-DMRs according to the combination of the
246 histone modification marks (see Methods). We found that promoter-distal hypo-DMRs were
247 significantly enriched by poised enhancer chromatin signatures (H3K4me1 without
248 H3K27me3) (Fisher's exact test, P <0.001) (Fig. 6e). Similarly, promoter-proximal hypo-

249 DMRs were enriched by bivalent promoters (H3K4me3 and H3K27me3) or active promoters
250 (H3K4me3) (Fisher's exact test, P = 3.80e-3, Active promoter; P= 7.36e-2, Bivalent) (Fig. 6f).
251 Thus, CHIP mutants appear to reprogram the epigenetic states including the loss of silent
252 marker at poised enhancers or bivalent promoters, which prime the IFN associated immune
253 response genes, thereby driving hyperinflammation and leading to the critical course of
254 COVID-19 (Fig. 7).

255

256

Discussion

By analyzing thorough clinical, radiological, and laboratory characteristics, as well as the presence of CHIP, we showed that CHIP is a novel risk factor for severe COVID-19 in previously healthy population without canonical clinical risk factors. scRNA-seq analysis revealed a distinct IFN-γ mediated immuno-pathogenic mechanism in CHIP (+) severe COVID-19 plausibly attributed by CHIP dependent chromatin reorganization. These results consistently indicate that CHIP may play a critical role in the progression of severe COVID-19, especially in previously healthy patients with its own immunologic pathway.

Exploration of an additional risk factor for severe COVID-19 is clinically valuable in this pandemic to predict the progression of COVID-19 more accurately and to improve our management strategy. Owing to its pro-inflammatory nature, CHIP may contribute to the progression of severe COVID-19. By analyzing more than 500 patients, Bolton *et al*. reported that CHIP is significantly associated with severe COVID-19[23], especially for patients carrying non-putative driver mutations. There have been a few controversial reports, however, they needed to be critically appraised because of methodological considerations. Duployez *et al.* showed a higher prevalence of CHIP in severe COVID-19 patients than age-matched hematologic malignancy-free cohort, but they could not show that CHIP affects clinical outcome[24]. However, they could only analyze severe patients whose clinical outcomes might hardly be differentiated by solely the presence of CHIP. In another study conducted by Hameister *et al.* involving 102 hospitalized patients with COVID-19, the presence of CHIP was not associated with severe COVID-19[25]. But the study lacked a stratified analysis or an adjustment for possible interactions. By introducing a hierarchical clustering, followed by thorough statistical examinations including interaction analysis, we could clearly show that CHIP is an independent risk factor for severe COVID-19.

281 COVID-19 patients were reported to show heterogeneous symptoms ranging from
282 asymptomatic to critical illness[3,44]. In line with it, many studies divided COVID-19 patients
283 into subgroups defined by immunological characteristics, for instance, patterns of sepsis[45],
284 subpopulations of lymphocytes[44], IFN responses in lung[46], or carrying loss-of-function
285 variants[47]. Single-cell techniques have been vigorously applied in COVID-19 to dissect
286 underlying causes of the diverse immune responses[33,48,49] and to elaborately determine the
287 relationship between immune subtypes and clinical characteristics[50,51]. Despite those important
288 works, none of the single-cell study has characterized the immunological effects of CHIP in
289 COVID-19 yet. In this regard, the current study uniquely demonstrated how CHIP-associated
290 somatic mutations in immune cells could actively establish a novel subgroup in COVID-19
291 patients. With single-cell immune transcriptome analysis, we could reveal that IFN-γ related
292 hyperinflammation is a hallmark of CHIP (+) severe COVID-19. Especially, there was an
293 enrichment of inflammatory signature in classical monocytes, which is compatible with recent
294 knowledge regarding the effect of CHIP on myeloid askew hematopoietic stem cell
295 differentiation[27]. From a cytokine perspective, IFN-γ and its synergism with TNF-α were
296 thought to play a critical role in the pathogenesis of severe COVID-19 in CHIP (+) patients.
297 This finding aligns with the previous report stating the role of IFN-γ and/or TNF-α in
298 exacerbating chronic inflammatory disease by CHIP[52]. Our study also implies that not only
299 type I IFN response but also type II IFN response plays an important role in disease
300 exacerbation in certain patients with severe COVID-19. Additional interesting immunological
301 finding reasonably explained with the CHIP biology is the up-regulation of genes related to
302 inflammatory macrophage in CHIP (+) severe COVID-19. CHIP is well known to drive
303 hyperinflammation in chronic disease mainly attributable to the altered function of monocyte
304 and macrophage [27].

305 Recent studies have revealed the pathological effects of CHIP such as atherosclerosis

306 and malignancy[18,53,54] and characterized the effect of CHIP mutations on hematopoiesis and
307 immunological functions regarding epigenetic mechanisms[55,56]. However, there is still an
308 ambiguity in how physiological pathogenic characteristics are linked to the altered chromatin
309 activities by CHIP mutations in actual patient cohorts. In our study, such linkage is explained
310 as regulatory interactions between pathogenic genes and their *cis*-regulatory elements with the
311 altered chromatin states, which are expected to be mediated by mutations in chromatin
312 regulators (Fig. 7). Although further investigation of other types of CHIP mutations such as
313 *TET2* and *ASXL1* are required to comprehensively characterize CHIP mutation-dependent
314 epigenetic reprogramming, the pathogenesis of other CHIP-dependent diseases could be
315 elucidated by considering the similar mechanisms.

316 There are several limitations in the present study. First, sample sizes of either entire
317 cohort or scRNA-seq-analyzed patients were limited. Second, the proportion of severe COVID-
318 19 was high in the present study since it was conducted mainly in tertiary-care hospitals.
319 Although we could show an apparent incline to severe COVID-19 in CHIP (+) patients and its
320 distinctive immune signature in this study, further validations in a larger prospective cohort
321 representing general COVID-19 patients are warranted. Third, scRNA-seq was performed with
322 PBMCs instead of lung fluid or infected lung tissues limiting our analysis in exploring systemic
323 inflammation as a result of COVID-19 pulmonary disease. Lastly, further studies are needed to
324 reveal the exact epigenetic differences between mutant and wild type monocytes in CHIP
325 patients and the real time point when CHIP mutant monocytes stir hyperinflammation.

326 Lastly, in terms of therapeutic strategy, Syk inhibitors have been implicated in
327 suppressing these pathogenic immune responses (Extended Data Fig. 5b) induced by CHIP. An
328 *in vitro* study on Syk inhibitor fostamatinib suggested its therapeutic effect against COVID-
329 19[57], and we have pending results of a randomized placebo-controlled trial with the drug

330 (NCT04579393). As the therapeutic efficacy of Syk inhibitors could be more potent in CHIP
331 (+) patients, it is worth evaluating treatment outcomes involving Syk inhibitors according to
332 CHIP status.

333 In summary, despite such limitations, we successfully clarified that there is a distinct
334 CHIP-driven severe COVID-19 subgroup and elucidated its unique immunological mechanism.
335 Revealing the underlying epigenetic mechanism for the altered immune function that aligns
336 with well-known CHIP biology suggests the robustness of our findings. It appears that classical
337 monocytes in patients with CHIP (+) COVID-19 undergo distinct immune responses, thus
338 focusing on immunomodulation strategies according to the presence of CHIP is required.
339 Considering the shared pathogenic host immune response across infections, we postulate that
340 our findings might bring a better understanding of previously unexplained exacerbation of
341 clinical conditions by various viruses.

342

343

344

345

Acknowledgments

We thank all our laboratory members for their support and critical suggestions throughout this work. Funding: This work was funded by the SUHF Fellowship (to I.J.). We also thank Dr. Shin for sharing specimens to determine the presence of CHIP.

Author Contribution

CKK, BC, YK, and IJ conceived the study. SP generated scRNA-seq data. AJL and YK generated Hi-C data. CKK, BC, SK, SHY, DL, and SK performed data analysis. CKK, EC, JJ, PGC, WBP, ESK, HBK, NJK, MO, SK, HI, JK, YHL, JL, JYL, JHM, and K-HS contributed to the collection of clinical information and samples. CKK, BC, YK, and IJ contributed to data interpretation with assistant from SK and KK. CKK and BC prepared the manuscript with assistance from YK and IJ. All authors read and commented on the manuscript.

References

1. World Health Organization. Novel Coronavirus (2019-nCoV) situation reports. (2020).
2. Zhu, N., *et al.* A Novel Coronavirus from Patients with Pneumonia in China, 2019. *N Engl J Med* **382**, 727-733 (2020).
3. Wu, Z. & McGoogan, J.M. Characteristics of and Important Lessons From the Coronavirus Disease 2019 (COVID-19) Outbreak in China: Summary of a Report of 72314 Cases From the Chinese Center for Disease Control and Prevention. *JAMA* **323**, 1239-1242 (2020).
4. Cunningham, J.W., *et al.* Clinical Outcomes in Young US Adults Hospitalized With COVID-19. *JAMA Intern Med* (2020).
5. Williamson, E.J., *et al.* Factors associated with COVID-19-related death using OpenSAFELY. *Nature* **584**, 430-436 (2020).
6. Zhang, S.Y., Zhang, Q., Casanova, J.L., Su, H.C. & Team, C. Severe COVID-19 in the young and healthy: monogenic inborn errors of immunity? *Nat Rev Immunol* **20**, 455-456 (2020).
7. Zhou, C., *et al.* Predictive factors of severe coronavirus disease 2019 in previously healthy young adults: a single-center, retrospective study. *Respir Res* **21**, 157 (2020).
8. Huang, C., *et al.* Clinical features of patients infected with 2019 novel coronavirus in Wuhan, China. *Lancet* **395**, 497-506 (2020).
9. Yang, X., *et al.* Clinical course and outcomes of critically ill patients with SARS-CoV-2 pneumonia in Wuhan, China: a single-centered, retrospective, observational study. *Lancet Respir Med* (2020).
10. Liu, Y., *et al.* Viral dynamics in mild and severe cases of COVID-19. *Lancet Infect Dis* (2020).
11. Zou, L., *et al.* SARS-CoV-2 Viral Load in Upper Respiratory Specimens of Infected Patients. *N Engl J Med* (2020).
12. Mehta, P., *et al.* COVID-19: consider cytokine storm syndromes and immunosuppression. *Lancet* **395**, 1033-1034 (2020).
13. Kang, C.K., *et al.* Aberrant hyperactivation of cytotoxic T-cell as a potential determinant of COVID-19 severity. *Int J Infect Dis* **97**, 313-321 (2020).
14. Xu, Z., *et al.* Pathological findings of COVID-19 associated with acute respiratory distress syndrome. *Lancet Respir Med* **8**, 420-422 (2020).
15. Merad, M. & Martin, J.C. Pathological inflammation in patients with COVID-19: a key role for monocytes and macrophages. *Nat Rev Immunol* **20**, 355-362 (2020).
16. Steensma, D.P., *et al.* Clonal hematopoiesis of indeterminate potential and its distinction from myelodysplastic syndromes. *Blood* **126**, 9-16 (2015).
17. Rodrigues, C.P., Shvedunova M., Akhtar A. Epigenetic Regulators as the Gatekeepers of Hematopoiesis. *Trends in Genetics* **37**(2021).
18. Jaiswal, S., *et al.* Clonal Hematopoiesis and Risk of Atherosclerotic Cardiovascular Disease. *N Engl J Med* **377**, 111-121 (2017).
19. Sano, S., *et al.* CRISPR-Mediated Gene Editing to Assess the Roles of Tet2 and Dnmt3a in

Clonal Hematopoiesis and Cardiovascular Disease. *Circ Res* **123**, 335-341 (2018).

20. Yura, Y., Sano, S. & Walsh, K. Clonal Hematopoiesis: A New Step Linking Inflammation to Heart Failure. *JACC Basic Transl Sci* **5**, 196-207 (2020).
21. Jaiswal, S. & Libby, P. Clonal haematopoiesis: connecting ageing and inflammation in cardiovascular disease. *Nat Rev Cardiol* **17**, 137-144 (2020).
22. Zekavat, S.M.*, et al.* Hematopoietic mosaic chromosomal alterations increase the risk for diverse types of infection. *Nat Med* **27**, 1012-1024 (2021).
23. Bolton, K.L.*, et al.* Clonal hematopoiesis is associated with risk of severe Covid-19. *medRxiv* (2020).
24. Duployez, N.*, et al.* Clinico-Biological Features and Clonal Hematopoiesis in Patients with Severe COVID-19. *Cancers (Basel)* **12**(2020).
25. Hameister, E.*, et al.* Clonal Hematopoiesis in Hospitalized Elderly Patients With COVID-19. *Hemasphere* **4**, e453 (2020).
26. Lee, J.S.*, et al.* Immunophenotyping of COVID-19 and influenza highlights the role of type I interferons in development of severe COVID-19. *Sci Immunol* **5**(2020).
27. Jaiswal, S. & Ebert, B.L. Clonal hematopoiesis in human aging and disease. *Science* **366**(2019).
28. Finak, G.*, et al.* MAST: a flexible statistical framework for assessing transcriptional changes and characterizing heterogeneity in single-cell RNA sequencing data. *Genome Biol* **16**, 278 (2015).
29. Duan, Q.*, et al.* LINCS Canvas Browser: interactive web app to query, browse and interrogate LINCS L1000 gene expression signatures. *Nucleic Acids Res* **42**, W449-460 (2014).
30. Angioni, R.*, et al.* Age-severity matched cytokine profiling reveals specific signatures in Covid-19 patients. *Cell Death Dis* **11**, 957 (2020).
31. Park, S.H.*, et al.* Type I interferons and the cytokine TNF cooperatively reprogram the macrophage epigenome to promote inflammatory activation. *Nat Immunol* **18**, 1104-1116 (2017).
32. Lucas, C.*, et al.* Longitudinal analyses reveal immunological misfiring in severe COVID-19. *Nature* **584**, 463-469 (2020).
33. Chua, R.L.*, et al.* COVID-19 severity correlates with airway epithelium-immune cell interactions identified by single-cell analysis. *Nat Biotechnol* **38**, 970-979 (2020).
34. Karki, R.*, et al.* Synergism of TNF-alpha and IFN-gamma Triggers Inflammatory Cell Death, Tissue Damage, and Mortality in SARS-CoV-2 Infection and Cytokine Shock Syndromes. *Cell* **184**, 149-168 e117 (2021).
35. Zhang, F.*, et al.* IFN-gamma and TNF-alpha drive a CXCL10+ CCL2+ macrophage phenotype expanded in severe COVID-19 lungs and inflammatory diseases with tissue inflammation. *Genome Med* **13**, 64 (2021).
36. Kang, K.*, et al.* IFN-γ selectively suppresses a subset of TLR4-activated genes and enhancers to potentiate macrophage activation. *Nat Commun* **10**, 3320 (2019).
37. Carvalho K., R.E., Jansen C., Williams K., Dowey A., McGill C., Mortazavi A. Uncovering the

439 Gene Regulatory Networks Underlying Macrophage Polarization Through Comparative
440 Analysis of Bulk and Single-Cell Data. *bioRxiv* (2021).
441 38. Liu, S.*, et al.* Critical role of Syk-dependent STAT1 activation in innate antiviral immunity. *Cell*
442 *Rep* **34**, 108627 (2021).
443 39. Li, S.*, et al.* Distinct evolution and dynamics of epigenetic and genetic heterogeneity in acute
444 myeloid leukemia. *Nat Med* **22**, 792-799 (2016).
445 40. Jung, I.*, et al.* A compendium of promoter-centered long-range chromatin interactions in
446 the human genome. *Nat Genet* **51**, 1442-1449 (2019).
447 41. Kim, K. & Jung, I. covNorm: An R package for coverage based normalization of Hi-C and
448 capture Hi-C data. *Comput Struct Biotechnol J* **19**, 3149-3159 (2021).
449 42. Zhang, J.*, et al.* An integrative ENCODE resource for cancer genomics. *Nat Commun* **11**,
450 3696 (2020).
451 43. Consortium, E.P. An integrated encyclopedia of DNA elements in the human genome. *Nature*
452 **489**, 57-74 (2012).
453 44. Mathew, D.*, et al.* Deep immune profiling of COVID-19 patients reveals distinct immunotypes
454 with therapeutic implications. *Science* **369**(2020).
455 45. Giamarellos-Bourboulis, E.J.*, et al.* Complex Immune Dysregulation in COVID-19 Patients with
456 Severe Respiratory Failure. *Cell Host Microbe* **27**, 992-1000 e1003 (2020).
457 46. Nienhold, R.*, et al.* Two distinct immunopathological profiles in autopsy lungs of COVID-19.
458 *Nat Commun* **11**, 5086 (2020).
459 47. Zhang, Q.*, et al.* Inborn errors of type I IFN immunity in patients with life-threatening COVID-
460 19. *Science* **370**(2020).
461 48. Liao, M.*, et al.* Single-cell landscape of bronchoalveolar immune cells in patients with COVID-
462 19. *Nat Med* **26**, 842-844 (2020).
463 49. Wilk, A.J.*, et al.* A single-cell atlas of the peripheral immune response in patients with severe
464 COVID-19. *Nat Med* **26**, 1070-1076 (2020).
465 50. Ren, X.*, et al.* COVID-19 immune features revealed by a large-scale single-cell transcriptome
466 atlas. *Cell* **184**, 1895-1913 e1819 (2021).
467 51. Stephenson, E.*, et al.* Single-cell multi-omics analysis of the immune response in COVID-19.
468 *Nat Med* **27**, 904-916 (2021).
469 52. Zhang, C.R.C.*, et al.* Inflammatory cytokines promote clonal hematopoiesis with specific
470 mutations in ulcerative colitis patients. *Exp Hematol* **80**, 36-41 e33 (2019).
471 53. Jaiswal, S.*, et al.* Age-related clonal hematopoiesis associated with adverse outcomes. *N Engl*
472 *J Med* **371**, 2488-2498 (2014).
473 54. Libby, P.*, et al.* Clonal Hematopoiesis: Crossroads of Aging, Cardiovascular Disease, and
474 Cancer: JACC Review Topic of the Week. *J Am Coll Cardiol* **74**, 567-577 (2019).
475 55. Izzo, F.*, et al.* DNA methylation disruption reshapes the hematopoietic differentiation
476 landscape. *Nat Genet* **52**, 378-387 (2020).
477 56. Zhang, Q.*, et al.* Tet2 is required to resolve inflammation by recruiting Hdac2 to specifically

repress IL-6. *Nature* **525**, 389-393 (2015).

57. Strich, J.R.*, et al.* Fostamatinib Inhibits Neutrophils Extracellular Traps Induced by COVID-19 Patient Plasma: A Potential Therapeutic. *J Infect Dis* **223**, 981-984 (2021).

482 **Figure Legends**

483 **Figure 1. Hierarchical clustering analysis for clinical characteristics of severe COVID-**
484 **19**

485 **a**, Overview of study design. **b**, A heatmap shows the hierarchical clustering result of clinical
486 characteristics. On the top, three different bars represent clusters and the presence of CHIP
487 mutations for each patient. The first bar represents two main clusters of patients (n=69 for
488 cluster A and n=74 for cluster B). The second bar represents five sub-clusters of patients
489 (n=32 for A1, n=18 for A2, n=19 for A3, n=47 for B1, and n=26 for B2). The third bar
490 represents the presence of CHIP. **c**, Boxplots showing clinical characteristics between cluster
491 A (orange) and B (green). For the boxplots, the box represents the interquartile range (IQR)
492 and the whiskers correspond to the highest and lowest points within 1.5 × IQR. Statistical
493 significance was examined with unpaired t-test (* < p-value 0.05, ** < p-value 0.01, and ***
494 < p-value 0.001). **d**, Barplots showing fractions of patients with comorbidities or CHIP for
495 cluster A1, A2, and A3. HTN stands for hypertension. DM stands for diabetes mellitus.
496

497 **Figure 2. Single-cell transcriptome analyses of COVID-19 according to CHIP status**
498 **a**, Scatter plots of integrated scRNA-seq data represented with a t-SNE method. Left, immunes
499 cells are presented according to the presence of CHIP. Others group indicates CHIP (-) COVID-
500 19 mild, influenza, and healthy normal control groups. Right, nine immune cell types were
501 plotted by a t-SNE method. **b**, A PCA analysis with transcriptome profiles according to the
502 immune cell types and disease groups. Colors and shapes represent the respective disease
503 groups or cell types. **c,** A scatter plot showing combined scores of LINCS L1000 Ligand
504 Perturbations up gene ontology library between CHIP (+) severe COVID-19 and CHIP (-)
505 severe COVID-19 compared to the healthy normal control. Identity lines are presented on
506 diagonal. Square of correlation of combined scores is shown together. **d-g**, Scatter plots

507 showing combined scores same gene ontology library in Fig. 2c for differentially expressed
508 genes between CHIP (+) and CHIP (-) severe COVID-19 in classical monocyte (d), CD4+ T
509 cell (e), non-classical monocyte (f), and IgG + B cell (g). The horizontal axis, up-regulated
510 genes in CHIP (+); Vertical axis, up-regulated genes in CHIP (-). Identity lines are presented
511 on diagonal. The color indicates types of perturbed ligand.

512

513 **Figure 3. CHIP specific immune signatures in classical monocytes**

514 **a**, Barplots showing combined scores of DEGs in classical monocytes between CHIP (+) and
515 CHIP (-) severe COVID-19 for same gene ontology library in Fig. 2c-g. The color indicates
516 up-regulated genes in CHIP (+) (green) and CHIP (-) (blue). Each point indicates one ligand
517 perturbation term in the library, in total 6 different types of ligands: IFN-α (n=5), IL-1β (n=6),
518 IFN-γ (n=6), IL-17 (n=2), IL-6 (n=2), TNF-α (n=6). The mean and standard error of the mean
519 (s.e.m) of each gene set are shown together. One-sided Mann-Whitney's U test was performed
520 (*: $P<0.05$, **: $P<0.01$). **b**, Barplots showing combined scores of same gene sets in Fig. 3a for
521 Ligand Perturbations from GEO up gene ontology library. The color indicates up-regulated
522 genes of CHIP (+) (pink) and CHIP (-) (yellow). **c**, Gene set enrichment analysis (GSEA) on
523 the same DEGs used in Fig. 3a-b for three classes of TLR induced genes[31]. Each plot shows
524 the distribution of enrichment of distinct class genes along with the list of the DEGs pre-ranked
525 with log-fold changes based on the CHIP (-) severe COVID-19. The color under the plot
526 indicates patient groups of up-regulated genes. Red, up-regulated in CHIP (+) severe COVID-
527 19. Blue, up-regulated in CHIP (-) severe COVID-19. Normalized enrichment scores (NES)
528 and FDR are shown together. Top, Class I genes. Middle, Class II genes. Bottom, Class III
529 genes.

530

531 **Figure 4. Pseudotime analyses of severe COVID-19 with CHIP in classical monocytes**

532 **a-c**, Pseudotime analyses for CHIP (+) or CHIP (-) severe COVID-19 patients. **a**, Cells are
533 aligned according to the pseudotime axis calculated by Monocle2. The color indicates a type
534 of cluster. Top, CHIP (+) patient. Bottom, CHIP (-) patient. **b**, Heatmaps representing the
535 expression level of marker genes for the ordered cells. The list of genes is the representative
536 gene set of each cluster. Barplots showing combined scores of each cluster for inflammatory
537 response term in MsigDB Hallmark 2020. **c**, Scatter plots of combined scores of marker genes
538 of inflammation clusters for LINCS L1000 Ligand Perturbations up gene ontology library. The
539 horizontal axis, high inflammation cluster; the vertical axis, low inflammation cluster. Identity
540 lines are presented on diagonal. Colors indicate types of perturbed ligand for IFN-α (n=5), IL-
541 1β (n=6), IFN- γ (n=6), IL-17 (n=2), IL-6 (n=2), TNF-α (n=6). Shapes represent the presence
542 or absence of CHIP. **d, e**, GSEA plots for marker genes of inflammation clusters in CHIP (+)
543 and CHIP (-), respectively. Genes are ordered based on log-fold changes between high
544 inflammation cluster and low inflammation cluster. Normalized enrichment scores (NES) and
545 FDR are presented for DEGs between M1-like (LPS-IFN-γ stimulated) and M0 macrophage
546 (untreated) [36](d) and DEGs between TNF-α-IFN-γ co-treatment and untreated condition[35] (e),
547 respectively. LPS indicates Lipopolysaccharide.

548

549 **Figure 5. Regulatory potential of CHIP-specific hypo-DMRs in IFN response genes**

550 **a,** Stacked bar plots showing the proportion of annotated hypo- and hyper-DMRs. In DMR,
551 Proximal to the promoter, n=1124; Distal regulatory element, n=423; others, n=801. In
552 random for DMR, Proximal to promoter, n=314; Distal regulatory element, n=81; others,
553 n=1953. **b**, Examples of CHIP (+) up-regulated genes are presented with hypo-DMRs and
554 multiple histone modification signatures for *FOXO3* (right) and *NFIL3* (left). **c,** Examples of

555 analysis of Hi-C data. Whole interaction map of chromosome 4 in 40kb resolution. The color
556 indicates normalized chromatin contact frequencies. Two example regions containing CHIP
557 (+) severe COVID-19 up-regulated genes in classical monocytes (region 1 and region 2) are
558 highlighted by yellow dashed lines. **d,** Hi-C contact maps (heatmap) for region 1 (*RBPJ*) and
559 region 2 (*CXCL2*) are shown together with significant long-range chromatin interactions with
560 the promoter regions (arcs on the below of the heatmap) and distribution of hypo-DMRs and
561 histone modifications signals. **e**, A pie chart showing proportions of hypo-DMR linked up-
562 regulated genes in CHIP (+) severe COVID-19 classical monocytes. The color indicates the
563 types of linkage between hypo-DMRs and up-regulated genes. **f**, **g**, Barplots of relative
564 combined scores to TNF-α of genes linked to hypo-DMRs and others for same gene ontology
565 library in Fig. 2c-g. Colors indicate types of perturbed ligands. Each point indicates one
566 ligand perturbation term. The mean and standard error of the mean (s.e.m) of each gene set
567 are presented in barplot. One-sided Mann-Whitney's U test was performed (n.s: non-
568 significant, **: $P<0.01$). Up-regulated genes in CHIP (+) compared to CHIP (-) (f) and
569 marker gens of high inflammation cluster compared to low inflammation cluster of CHIP (+)
570 patient in Fig. 4 (g).
571

572 **Figure 6. Chromatic states of hypo-DMRs linking to CHIP specifically up-regulated**
573 **genes**
574 **a, b**, CHIP-seq signal distribution (a for H3K27ac and b for H3K27me3) of 20k upstream and
575 downstream surrounding of hypo-DMRs (n=1,693), hyper-DMRs (n=655) and randomly
576 selected regions. Each randomly selected regions have the same distribution of chromosome
577 number and length of hypo- and hyper-DMR, respectively. Top, average ChIP-seq signal
578 distributions. Bottom, heatmaps of CHIP-seq signals of the corresponding regions. **c, d,** CHIP-

seq signal distribution for CHIP (+) up-regulated genes linked (n=209) and unliked (n=1484) hypo-DMRs for H3K4me1 (c) and H3K4me3 (d). Top, average profiles of CHIP-seq signals for linked and unlinked hypo-DMRs. Bottom, heatmaps of CHIP-seq signals of the corresponding regions. **e**, **f**, Stacked barplots of the linked and unlinked hypo-DMRs with annotation of chromatin states. For statistical significance, one-sided Fisher's exact test was performed between linked and unlinked for promoter-distal (e) or -proximal (f) hypo-DMRs.

Figure 7. A proposed model for the pathogenesis of severe COVID-19 in patients with CHIP

A schematic overview shows the progression of disease exacerbation in terms of gene regulation, cellular level, and clinical/immunological signatures under CHIP (+) severe COVID-19.

591 **Extended Data Figure 1. A heatmap showing hierarchical clustering of severe COVID-19**
592 **patients with comorbidities and CHIP.**

593 The first bar represents two clusters, cyan for non-CHIP enriched (n=65), and orange for CHIP
594 enriched one (n=25). The second bar represents five distinct types of sub-clusters, namely, red,
595 for without comorbidity (n=19), orange for DM (n=9), green for HTN (n=26), purple for CHIP
596 (n=13), and blue for complex (n=23). The color in the heatmap represents the presence of CHIP.

597

598 **Extended Data Figure 2. Quality-control and cell-type annotation of single-cell RNA-seq**
599 **results**

600 **a, b,** Scatter plots showing CHIP (+) patients' immune cells according to the UMI count and
601 other features. Percentage of the mitochondrial genes (a) and the number of detected genes (b).
602 **c,** Scatter plot of log 10-transformed count data between individual patients. R represents
603 Pearson's correlation coefficient values. **d,** t-SNE clusters of integrated single-cell data. **e,** Each
604 cell type marker gene expression on t-SNE plot. **f**, Stacked barplots show cell-type proportions
605 of each patient group. **g**, Boxplots showing the ratio of the proportion of classical monocytes.
606 (left) All pairs within CHIP (+) patients (n=30). (right) all pairs between CHIP (+) and CHIP
607 (-) (n=18). The box represents the interquartile range (IQR) and the whiskers correspond to the
608 highest and lowest points within 1.5 × IQR. Two-sided Kolmogorov-Smirnov test were
609 performed (** < p-value 0.01).

610

611 **Extended Data Figure 3. Analyses of differently expressed genes between CHIP (+) severe**
612 **COVID-19 and other groups**

613 **a**, Chow-ruskey venn diagram of the up-regulated genes in CHIP (+) severe COVID-19

614 compared to other disease groups. The color of the border in diagrams represents five immune
615 cell types. Monocyte (red), classical monocyte and non-classical monocyte; natural killer T
616 cells (orange); $CD4^+$ T cell (green), $CD4^+$ T cell and $CD4^+$ naïve T cell; $CD8^+$ T cell (blue),
617 $CD8^+$ T cell and $CD8^+$ memory T cells; B cell (purple), IgG^+ B cell and IgG^- B cell. **b**, Barplots
618 showing combined scores for gene ontology terms in MsigDB Hallmark 2020 with up-
619 regulated genes in CHIP(+) severe COVID-19. Top six terms were presented. The color
620 indicates normal or disease controls. **c**, Ratio of cell-type specific CHIP (+) severe COVID-19
621 up-regulated genes compared to total up-regulated genes for comparison with other disease
622 groups. The mean and standard error of the mean (s.e.m) of each gene set are presented in
623 barplots. The color indicates the type of disease group for comparison.

624

625 **Extended Data Figure 4. Enriched immune signatures in CHIP (+) and CHIP (-) severe**
626 **COVID-19 up-regulated genes compared to healthy normal control**

627 **a-e**, Scatter plots showing combined scores of differentially expressed genes (DEGs) in
628 selected cell types between severe COVID-19 patient groups for same gene ontology library in
629 Fig. 2c. The horizontal axis, up-regulated genes in CHIP (+) patients; the vertical axis, up-
630 regulated genes in CHIP (-) patients. Identity lines are presented on diagonal. The color
631 indicates types of perturbed ligand in database terms. **a**, CD8+ T cell. **b**, CD8+ memory T cell.
632 **c**, IgG- B cell. **d**, CD4+ naive T cell. **e**, Natural killer T cell.

633

634 **Extended Data Figure 5. An inflammatory macrophage signature in CHIP (+) classical**
635 **monocytes in severe COVID-19**

636 **a,** GSEA plots for marker genes of inflammation clusters in CHIP (+) and CHIP (-), respectively.
637 Genes are ordered based on log-fold changes between high inflammation cluster and low
638 inflammation cluster. Normalized enrichment scores (NES) and FDR are presented for DEGs
639 between M1-like and M0 macrophage[37]. **b**, the effect of SYK inhibitor to suppress CHIP (+)
640 up-regulated genes. Comparison between combined scores of marker genes of high
641 inflammation cluster for Kinase Perturbations from GEO down gene ontology library for
642 inhibitors or knock out of SYK kinase terms. One-sided Paired t-test was performed (*: $P<$
643 0.05).

644

645 **Extended Data Figure 6. The distribution of the nearest distance between differently**
646 **expressed gene promoters and DMRs**

647 Boxplots of the nearest distance between differentially expressed genes (right: CHIP (+) up-
648 regulated genes, left: CHIP (-) up-regulated genes) and DMRs. Hypo-DMRs were randomly
649 selected to have the same sample size as hyper-DMRs. The box represents the interquartile
650 range (IQR) and the whiskers correspond to the highest and lowest points within 1.5 × IQR.
651 The color indicates the types of DMRs. Distance is represented as the log scale, with a 10kb
652 resolution. For statistical significance test, two-sided Kolmogorov-Smirnov test were
653 performed between hypo- and hyper-methylated regions ($P<0.001$, CHIP (+); $P=3.46e-3$, CHIP
654 (-)).

Kang et al Figure 1

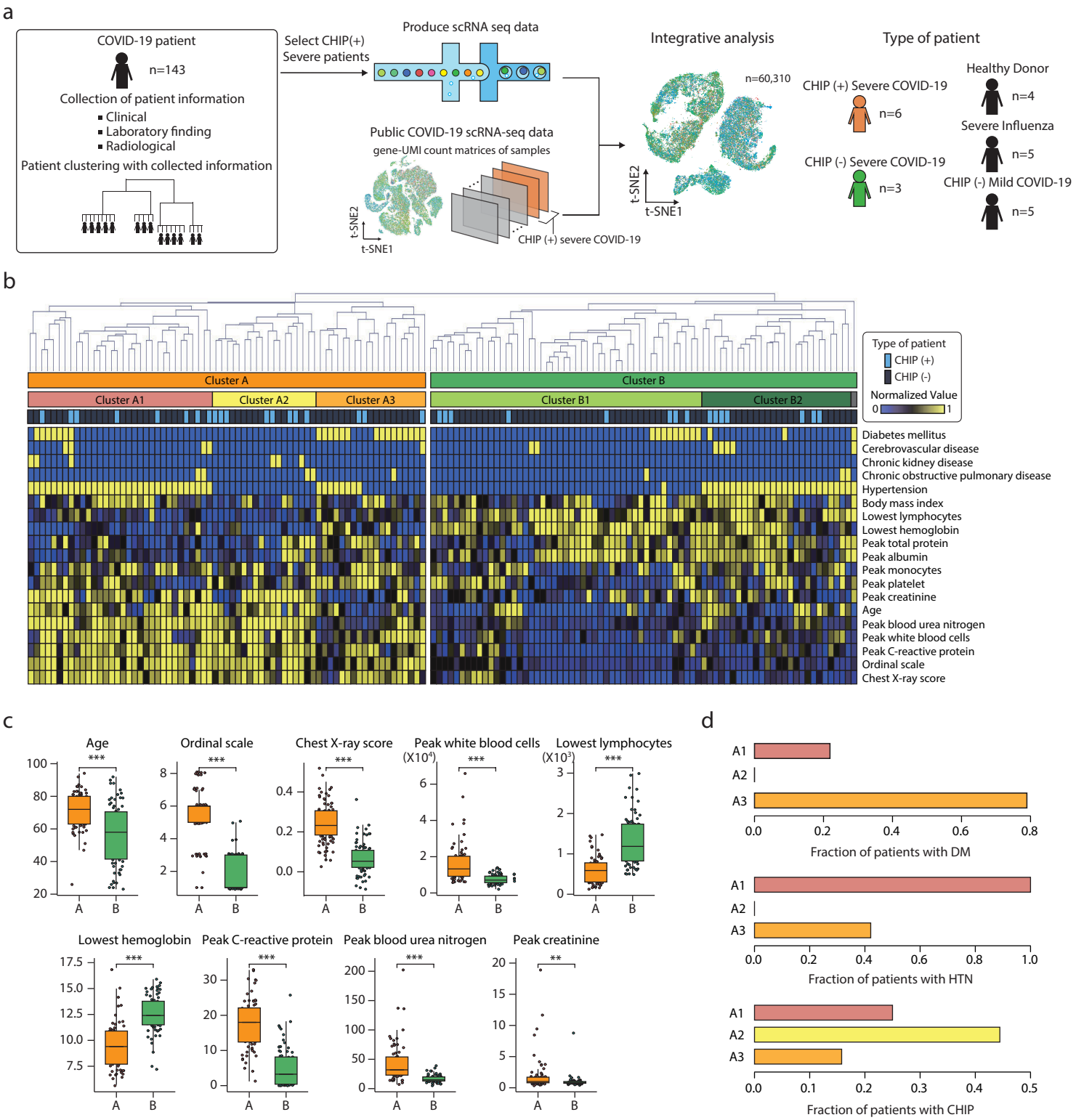

Kang et al Figure 2

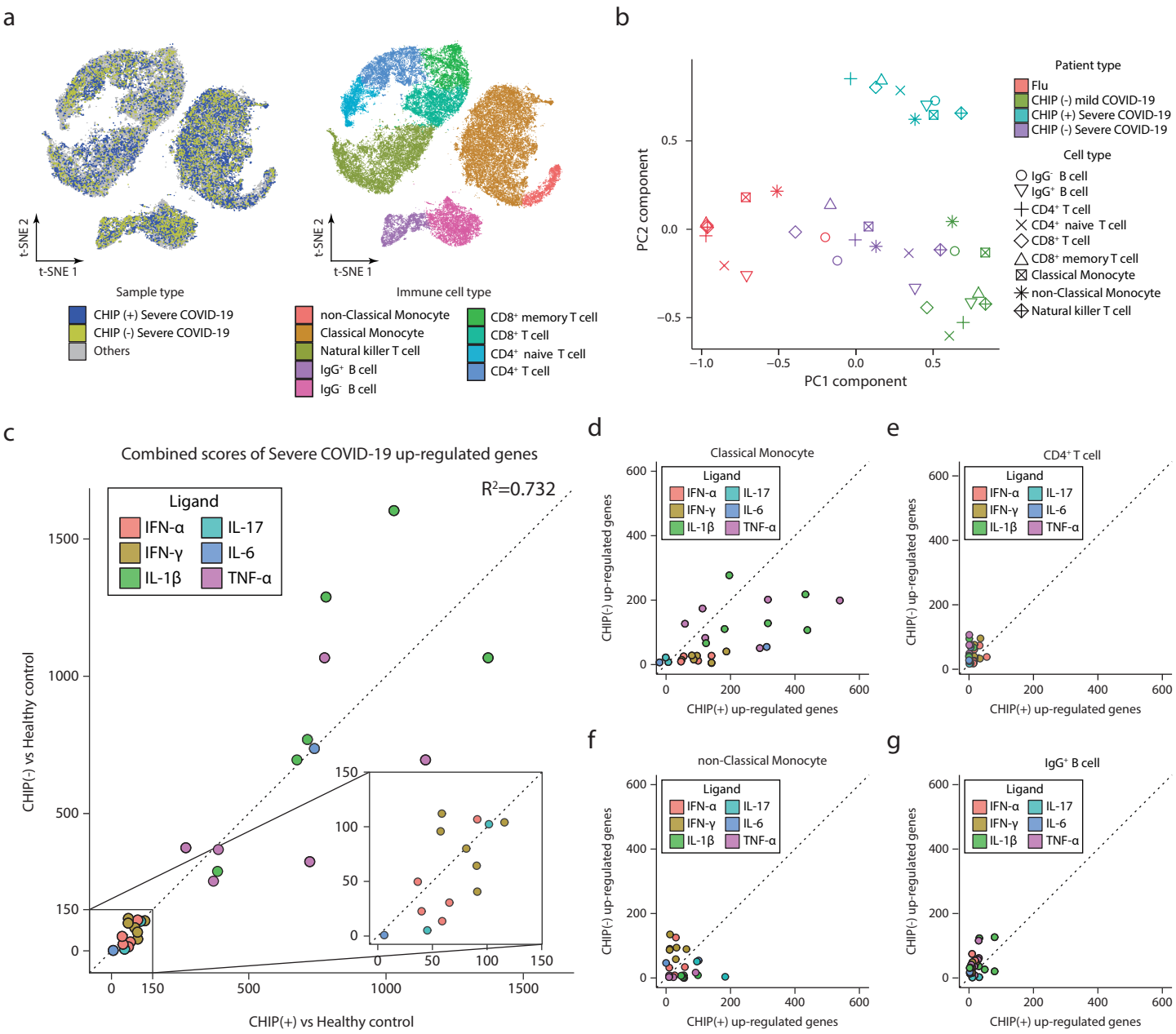

Kang et al Figure 3

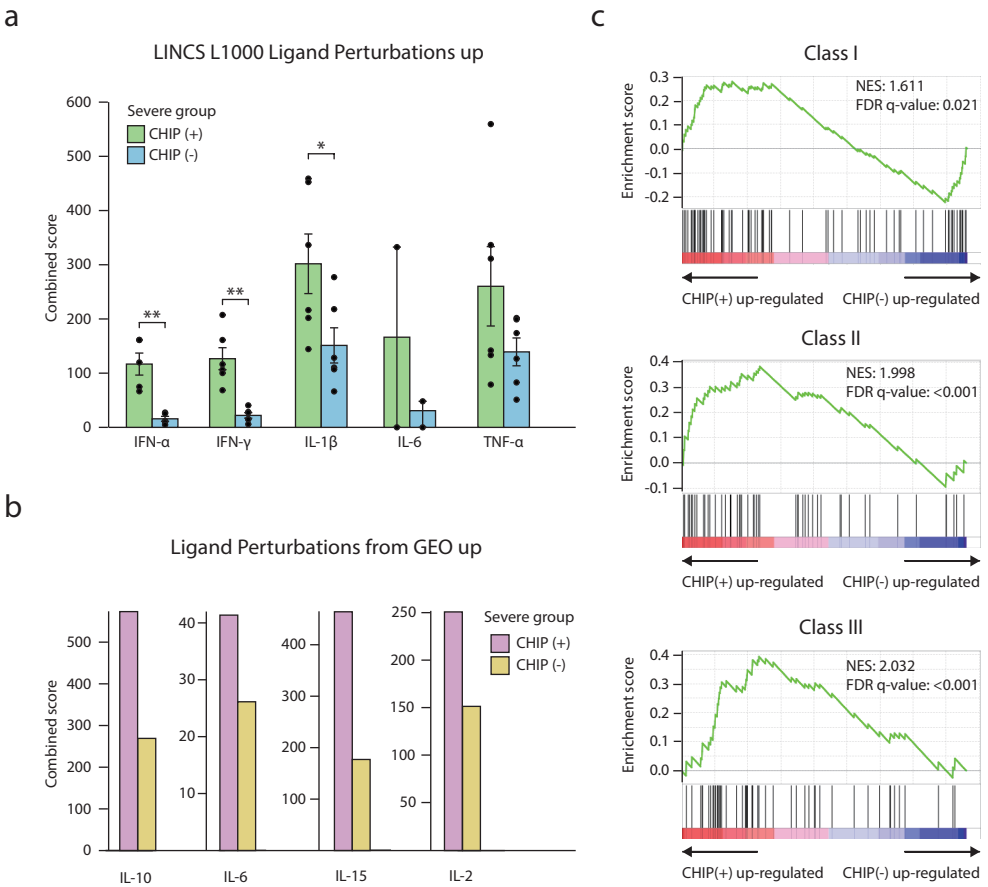

Kang et al Figure 4

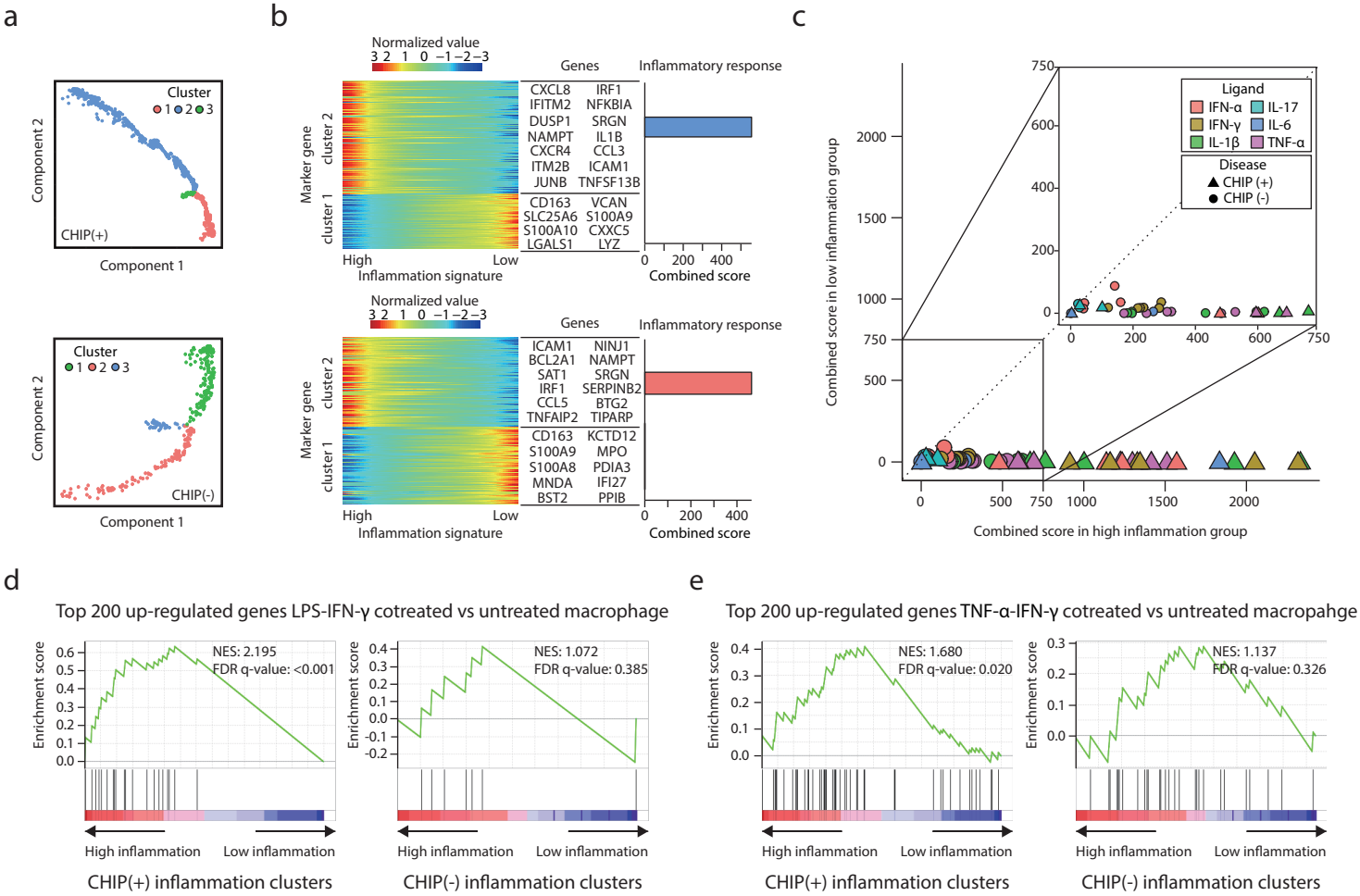

Kang et al Figure 5

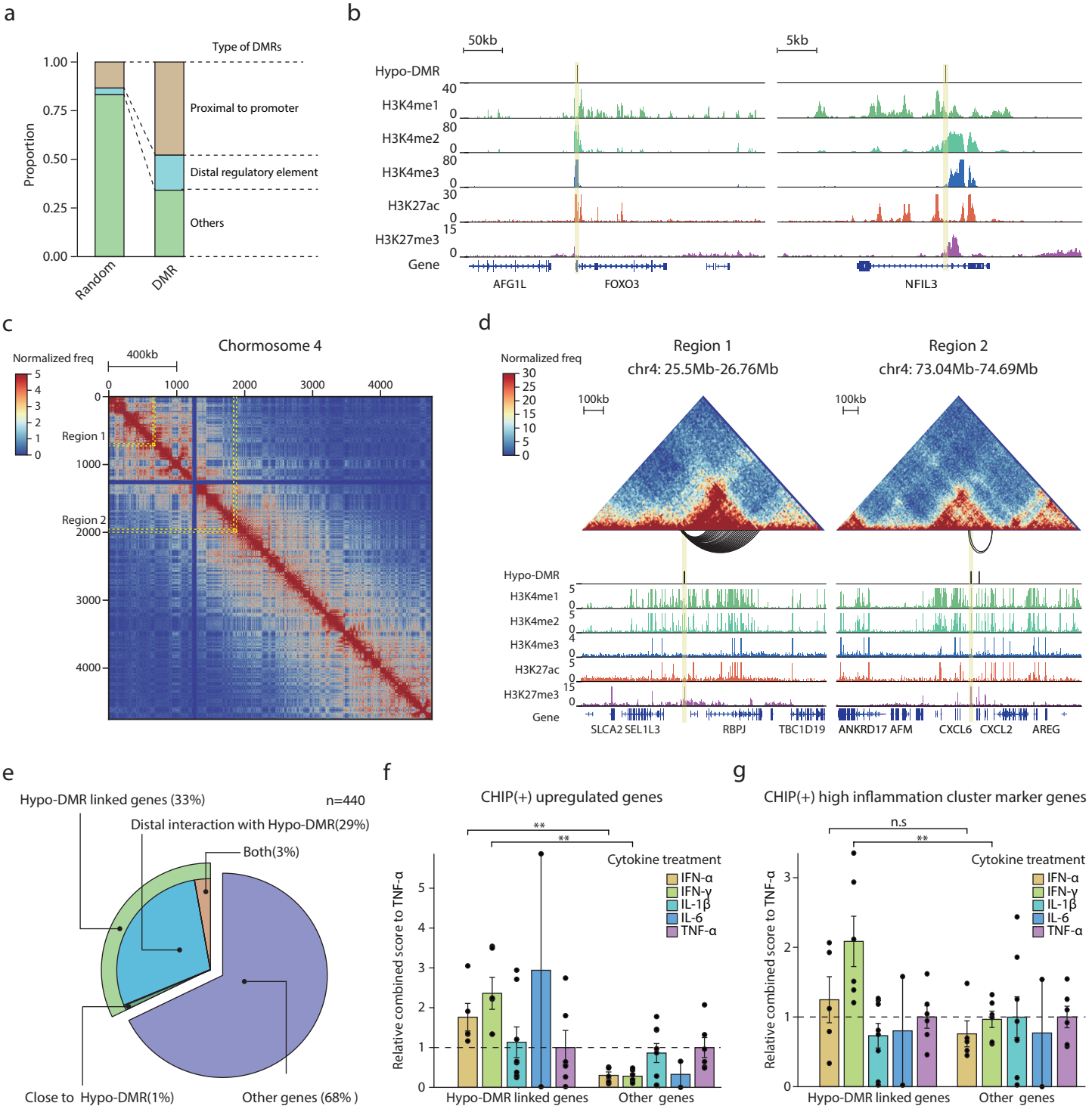

Kang et al Figure 6

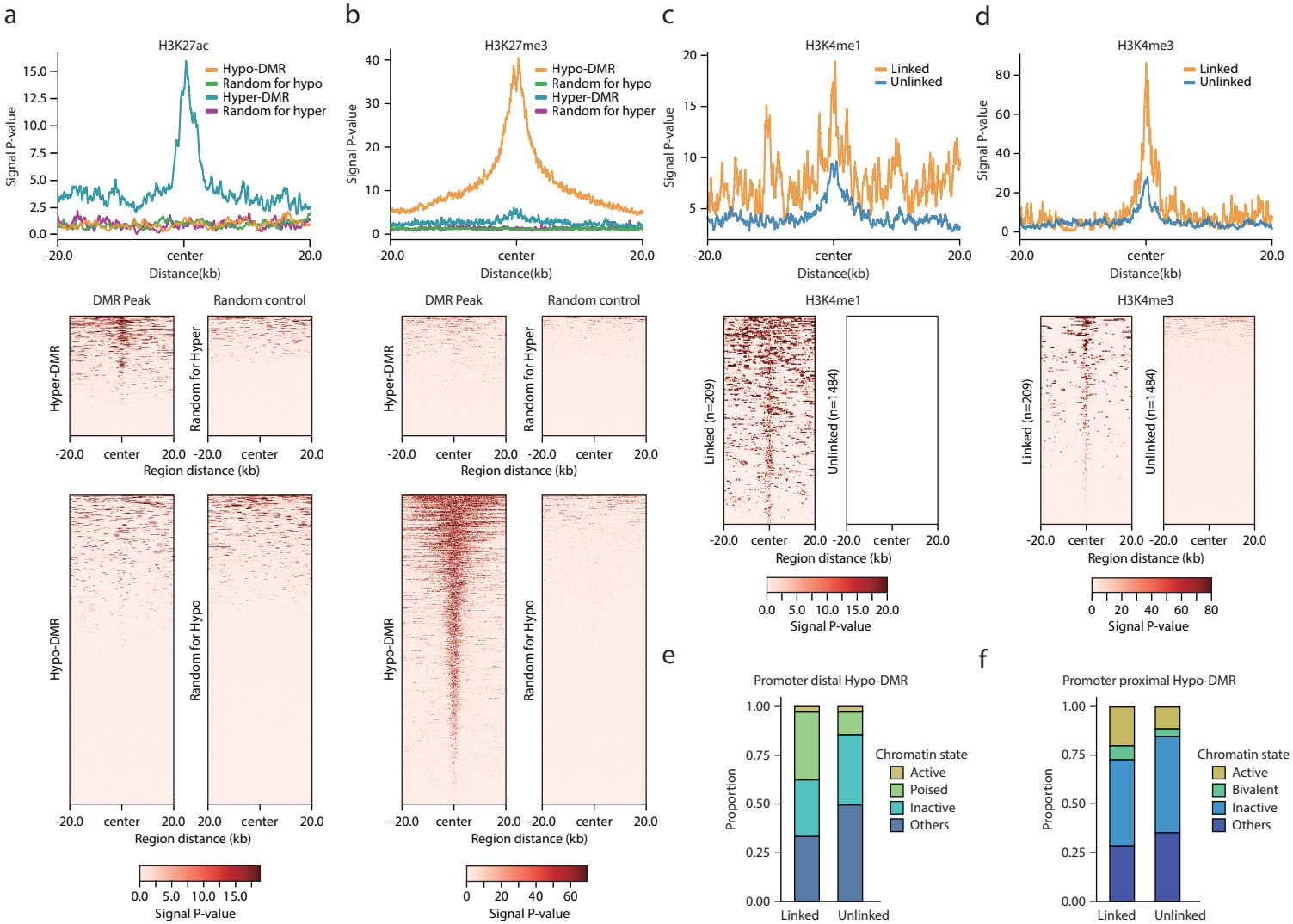

Kang et al Figure 7

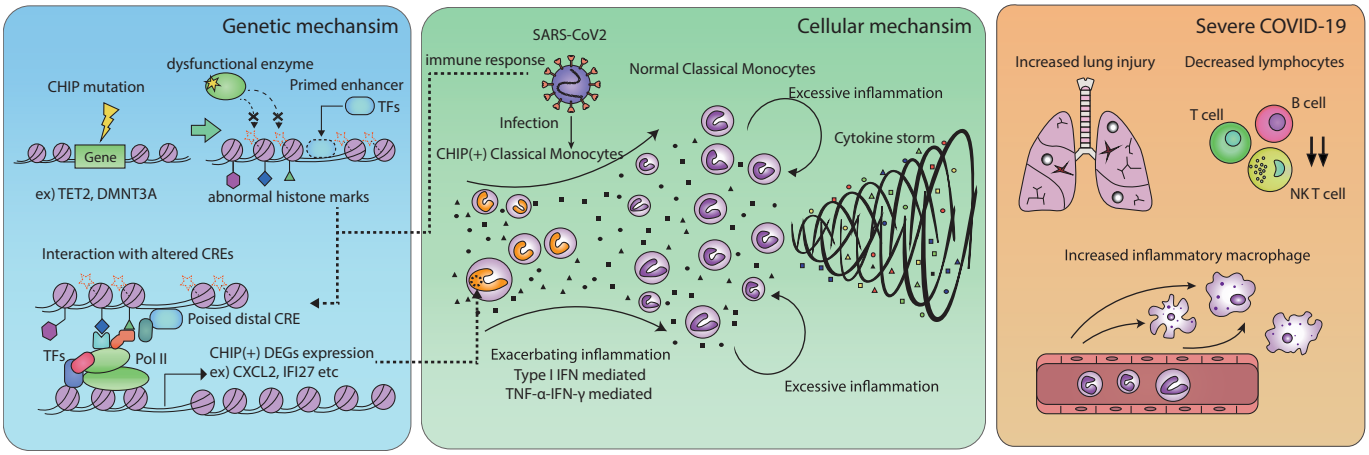

Kang et al Extended Data Figure 1

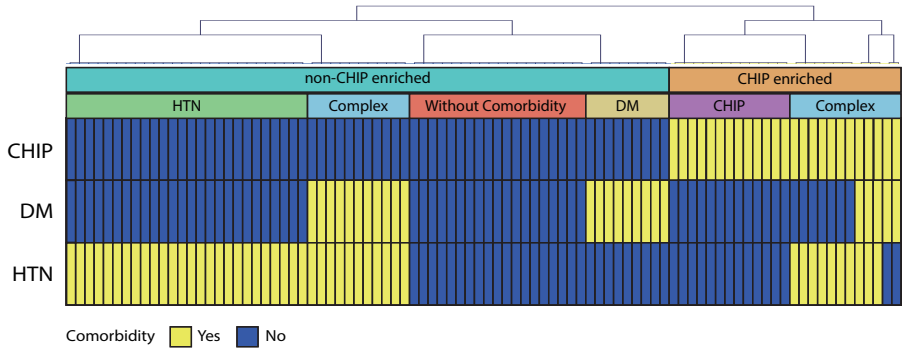

Kang et al Extended Data Fig 2

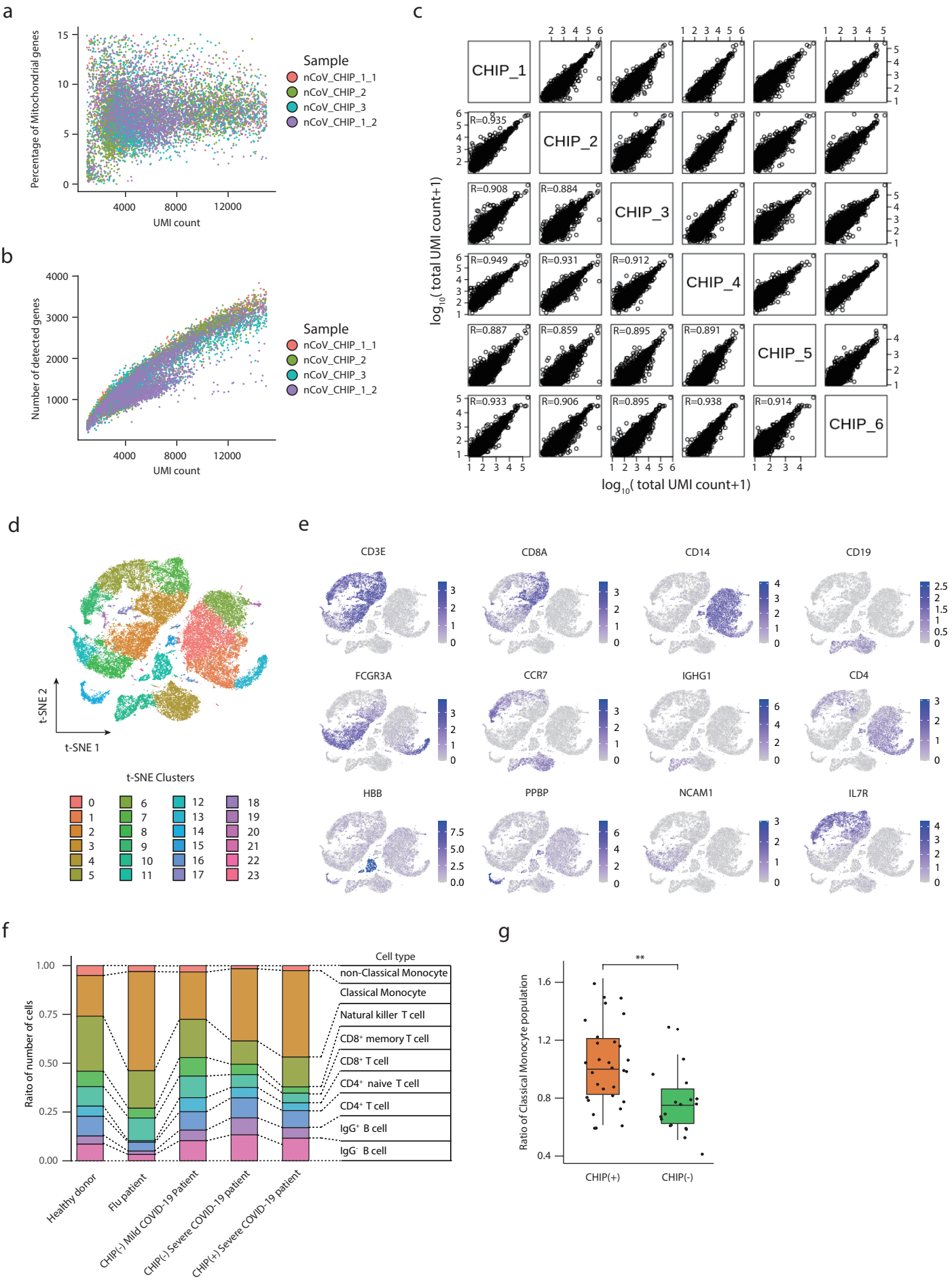

Kang et al Extended Data Fig 3

a

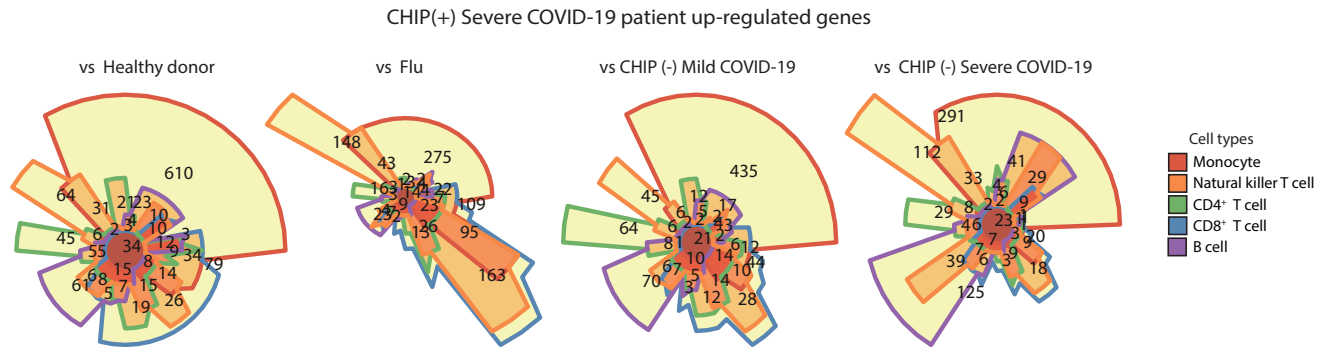

b

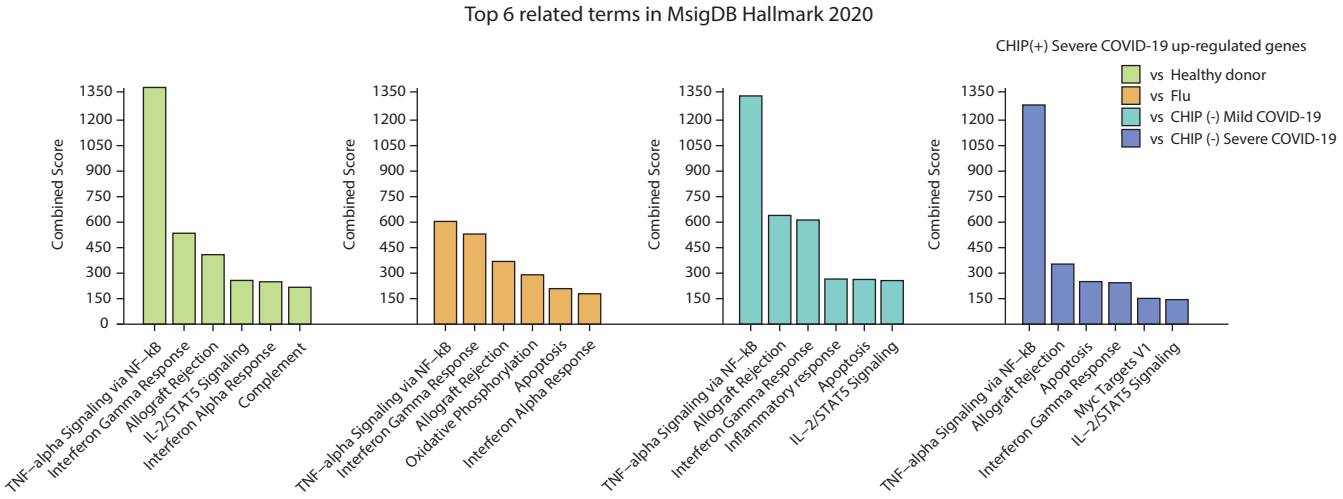

c

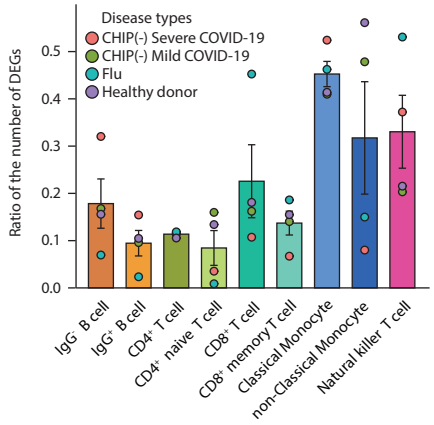

Kang et al Extended Data Fig 4

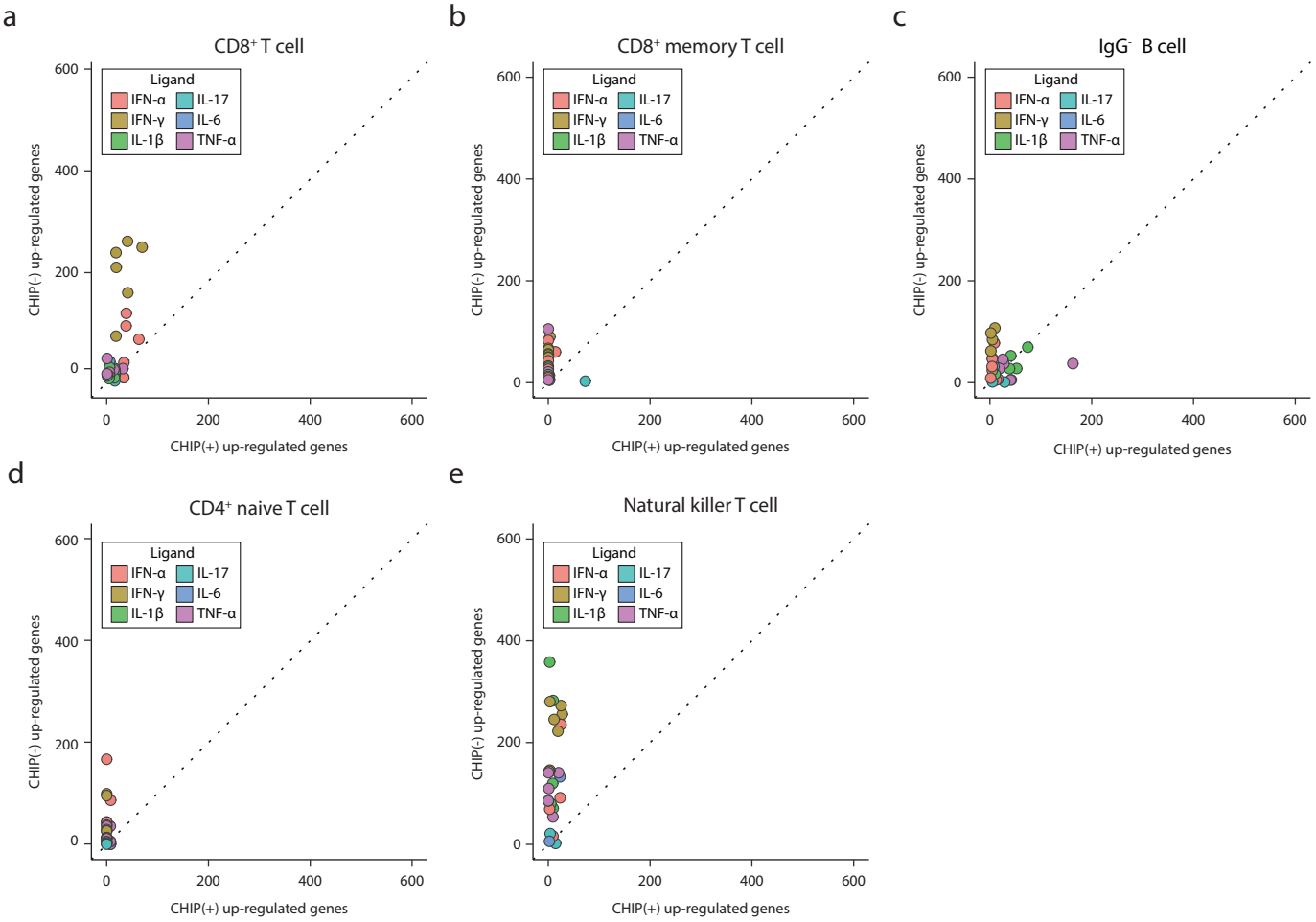

Kang et al Extended Data Fig 5

a

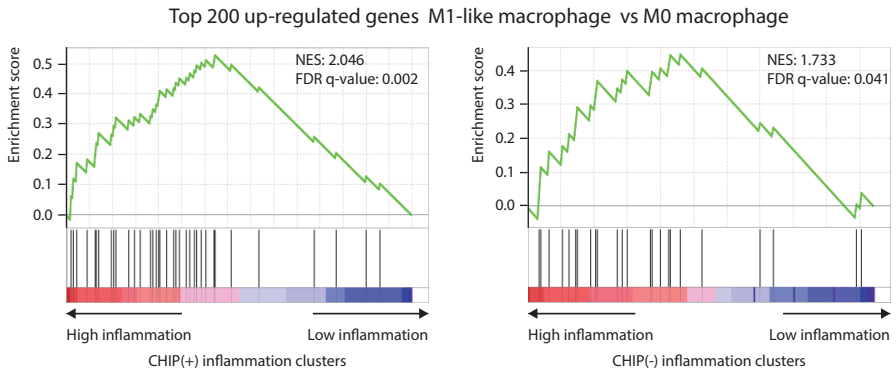

b

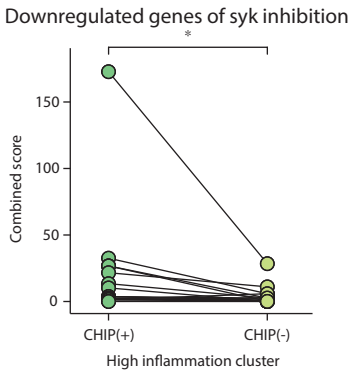

Kang et al Extended Data Fig 6

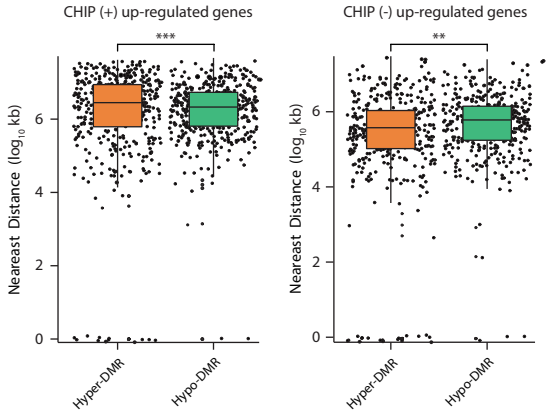

655 **Tables**

656 **Table 1. Age and gender-adjusted odds ratio of the presence of CHIP for severe COVID-**
657 **19 in canonical risk factors-stratified subgroups**

658 **Table 2. Final multivariate model for independent risk factors for severe COVID-19**
659 **including interaction term between CHIP and canonical risk factors**

660

661 **Supplementary Tables**

662 **Supplementary Table 1. Baseline characteristics of COVID-19 patients in this study**
663 **according to the presence or absence of clonal hematopoiesis of indeterminate potential**

664 **Supplementary Table 2. Clinical characteristics of cluster A2 when compared other cases**
665 **in cluster A**

666 **Supplementary Table 3. Clinical information of patient used in scRNA seq**

667 **Supplementary Table 4. Data quality of scRNA seq**

668 **Supplementary Table 5. A list of DMRs**

669

670

671

672

673

674

675

676 **Table 1. Age and gender-adjusted odds ratio of the presence of CHIP for severe COVID-**

677 **19 in canonical risk factors-stratified subgroups**

	Severe COVID-19		**aOR (95% CI)**	***P***
	CHIP (+)	CHIP (-)		
Canonical risk factor present	13/21 (61.9%)	47/68 (69.1%)	0.4 (0.1—1.4)	0.159
Canonical risk factor absent	12/13 (92.3%)	18/41 (43.9%)	14.8 (1.3—164.1)	0.028
Total	25/34 (73.5%)	65/109 (59.6%)	1.1 (0.4—2.8)	0.829

678 CHIP, clonal hematopoiesis with indeterminate potential; aOR, adjusted odds ratio; CI,

679 confidence interval

680 Canonical risk factors were BMI ≥ 30.0, diabetes mellitus, and hypertension.

681

682

683

684

685

686

687

688

689

690

691 **Table 2. Final multivariate model for independent risk factors for severe COVID-19**

692 **including interaction term between CHIP and canonical risk factors**

	aOR	*P*
Age, per one year	1.1 (1.0—1.1)	< 0.001
Male gender	2.0 (0.9—4.5)	0.075
CHIP	10.7 (1.1—100.7)	0.038
Canonical risk factors	2.0 (0.8—5.0)	0.120
CHIP * conventional risk factors	0.0 (0.0—0.5)	0.012

693 CHIP, clonal hematopoiesis with indeterminate potential; aOR, adjusted odds ratio

694 Canonical risk factors were BMI ≥ 30.0, diabetes mellitus, and hypertension.

695

696

697

698

699

700

701

702

703

704